Stereoselective synthesis, structure and DFT studies on fluoro- and nitro- substituted spirooxindole-pyrrolidine heterocyclic hybrids

A.I. Almansour, N. Arumugam, S.M. Soliman, B.S. Krishnamoorthy, J.-F. Halet, R.V. Priya, J. Suresh, D.M. Al-Thamili, F.A. Al-Aizari, R.S. Kumar

▶ **To cite this version:**

A.I. Almansour, N. Arumugam, S.M. Soliman, B.S. Krishnamoorthy, J.-F. Halet, et al.. Stereoselective synthesis, structure and DFT studies on fluoro- and nitro- substituted spirooxindole-pyrrolidine heterocyclic hybrids. Journal of Molecular Structure, 2021, 1237, pp.130396. 10.1016/j.molstruc.2021.130396 . hal-03225472

HAL Id: hal-03225472
https://hal.science/hal-03225472

Submitted on 11 Jun 2021

HAL is a multi-disciplinary open access archive for the deposit and dissemination of scientific research documents, whether they are published or not. The documents may come from teaching and research institutions in France or abroad, or from public or private research centers.

L'archive ouverte pluridisciplinaire **HAL**, est destinée au dépôt et à la diffusion de documents scientifiques de niveau recherche, publiés ou non, émanant des établissements d'enseignement et de recherche français ou étrangers, des laboratoires publics ou privés.

Journal Pre-proof

Highlights

- Structurally diverse spirooxindole-pyrrolidine molecular scaffolds achieved.
- Their molecular structures were elucidated from NMR, X-ray and DFT studies.
- Hirshfeld analysis was performed to determine different intermolecular contacts.
- DFT computed parameters are in good agreement with experimental findings.

Journal Pre-proof

Stereoselective synthesis, structure and DFT studies on fluoro- and nitro- substituted spirooxindole-pyrrolidine heterocyclic hybrids

Abdulrahman I. Almansour,[1] Natarajan Arumugam,[1] Saied M. Soliman,[2] Bellie Sundaram Krishnamoorthy,[3,4] Jean-Francois Halet,[4] R. Vishnu Priya,[5] J. Suresh,[5] Dhaifallah M. Al-thamili,[1] Faiz A. Al-aizari,[1] and Raju Suresh Kumar[1,*]

[1]*Department of Chemistry, College of Science, King Saud University, P.O. Box 2455, Riyadh 11451, Saudi Arabia*
[2]*Department of Chemistry, Faculty of Science, Alexandria University, P.O. Box 426, Ibrahimia, Alexandria 21321, Egypt*
[3]*Department of Chemistry, Vivekanandha College of Arts and Sciences for Women (Autonomous), Elayampalayam, Namakkal, Tamil Nadu 637 205, India*
[4]*Institut des Sciences Chimiques de Rennes, UMR 6226, CNRS-Universite´ de Rennes 1, 35042 Rennes Cedex, France*
[5]*Department of Physics, The Madhura College, Madurai, 625 011, India*

Journal Pre-proof

Graphical abstract

Structurally diverse highly functionalized flouro- and nitro- substituted spirooxindole-pyrrolidine molecular scaffolds have been achieved and their molecular structures were elucidated by NMR spectroscopy and X-ray crystallographic studies. Geometric parameters calculated by DFT are in good agreement with the experimental data obtained from the X-ray crystallography.

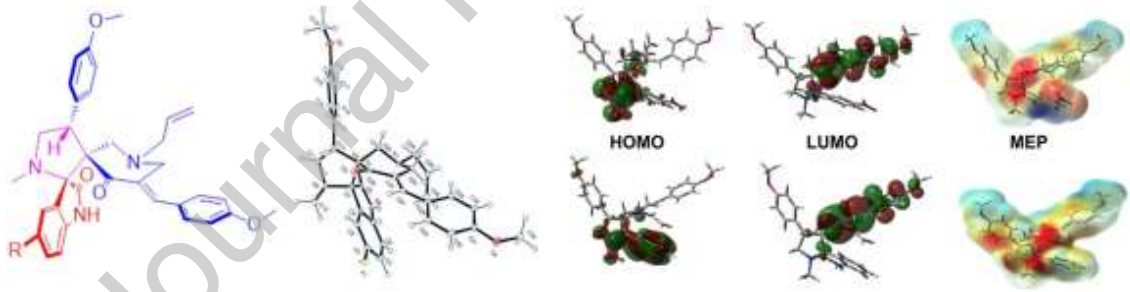

Abstract

Structurally diverse highly functionalized flouro- and nitro- substituted spirooxindole-pyrrolidine heterocyclic hybrids have been achieved in good yields. The molecular structure of these diverse spiroheterocyclic hybrids was elucidated by spectroscopic analysis and further confirmed by single crystal X-ray crystallographic studies and Density Functional Theory (DFT) calculations. Analysis of molecular packing for these hybrids was performed using Hirshfeld analysis. Geometric

*Corresponding author: email: sraju@ksu.edu.sa, drrajusureshkumar@gmail.com (Suresh Kumar R).

parameters calculated by DFT are in good agreement with the experimental data obtained from X-ray crystallography.

Keywords: [3+2] Cycloaddition; fluoro- nitro- spirooxindole-pyrrolidine; Ionic liquid; single crystal; DFT studies.

Journal Pre-proof

1. Introduction

Multicomponent reactions (MCR) received much attention from the research community in recent years due to their efficient and atom economic process. Although the first MCR reaction (Strecker Synthesis) has been reported 150 years back, many MCR reactions (Biginelli Reaction, Mannich Reaction, etc.) ie., multi-component one pot synthesis of organic molecules are reported extensively for the past two decades. In specific, design and construction of organic heterocyclic hybrids through multicomponent reactions employing nonconventional solvents is the prime target for organic chemists as this phenomenon has been accepted to be green. Many of the heterocyclic hybrids obtained from one pot MCR are showing important applications in biological and/or pharmaceutical area [1]. Pyrrolidines, an attractive five membered ring amines, are the central moiety present in diverse natural and synthetic compounds, can be constructed through the [3+2] cycloaddition reactions of azomethine ylides with olefinic dipolarophiles [2]. Spiropyrrolidines have important applications in drug industry as potential antileaucamic, anticonvulsant agents and possess antiviral and local anesthetic activities. Whilst, spirooxindoles gain noteworthy consideration due to its exceptional structural features and distinct biological activities [3-6]. The spirooxindole-pyrrolidine central moiety is the core unit in many alkaloids [7-9] possessing antibacterial, antifungal, antimalarial, antidiabetic and antimycobacterial activities. Due to their diverse structural features and biological significance, the effective green synthesis of these hybrid architectures is the prime target of our group.

Ionic liquids are well recognized for their high chemical and thermal stability, solvating ability, behavior as acidic, basic catalysts and recyclability. These fascinating properties makes them an environmentally friendly medium [10] for many organic transformations. Although many ionic liquids are known and being used, 1-butyl-3-methylimidazolium bromide, [bmim]Br has been considered to be one of the efficient reaction medium for [3+2] cycloaddition reactions [11-14] leading to the formation of spiropyrrolidines.

In continuation of our research interest towards the synthesis and/or biological potential of novel hybrid heterocycles [15-24], herein we report a simple and facile construction of fluoro- and nitro- substituted spirooxindole-pyrrolidine central moiety *via* the [3+2] cycloaddition of azomethine ylide generated *in situ* from 4-fluoroisatin/4-nitroisatin and sarcosine to (3*E*,5*E*)-1-allyl-3,5-bis(4-methoxyphenylmethylidene)piperidin-4-one in an ionic liquid, [bmim]Br. The molecular structure of these compounds is elucidated by NMR spectroscopy and further confirmed

by X-ray diffraction and DFT studies. DFT calculations were being used to predict the electronic properties and reactivity descriptors of these compounds.

2. Materials and methods

Experimental

2.1. Chemistry

Melting points were recorded using open capillary tubes and are uncorrected. The ^{1}H and ^{13}C NMR spectra were recorded on a Bruker400 or 500 MHz instruments (Faellanden, Switzerland) in $CDCl_3$ using TMS as internal standard. Standard Bruker software was used throughout. Chemical shifts are given in parts per million (δ-scale) and the coupling constants are given in Hertz. Elemental analyses were performed on a Perkin Elmer 2400 Series II Elemental CHNS analyzer (Waltham, MA, USA).

2.1.1. General procedure for the synthesis of 6

An equimolar mixture of N-allyl-bismethoxyphenylmethylidene-piperidone **3** (1 mmol), isatin **4(a,b)** (1.1 mmol) and sarcosine **5** (1.1mmol), in 200 mg of [bmim]Br was heated with constant stirring at 100 ^{o}C for 30 minutes. After the reaction was complete as noticeable from TLC, 50 mL of water was added to the reaction mixture and extracted with ethyl acetate (3x30 mL). The solid obtained was dried in vacuum and purified through column chromatography using hexane: ethyl acetate (3:2 v/v) as eluent to obtain the product as colorless solid in good yields.

2.1.2. Spiro[2.3″]5″-nitrooxindole-spiro[3.3′]-1′-allyl-5′-(4-methoxyphenylmethylidene)-tetrahydro-4′(1H)-pyridinone-4-(4-methoxyphenyl)-pyrrolidine (6a)

Mp: 182-183 °C; ^{1}H NMR (500 MHz, $CDCl_3$): δ_H 1.82 (d, 1H, *J* = 13.0 Hz, 2'-CH_2), 2.14, (s, 3H, N-CH_3), 2.72 (dd, 1H, *J* = 13.0, 8.0 Hz, 7'-CH_2), 2.88 (dd, 1H, *J* = 14.5, 2.5 Hz, 6'-CH_2), 3.01-3.06 (m, 1H, 7'-CH_2), 3.24 (dd, 1H, *J* = 13.0, 1.5 Hz, 2'-CH_2), 3.36-3.39 (m, 1H, 5-CH_2), 3.43 (d, 1H, *J* = 14.5 Hz, 6'-CH_2), 3.78 (s, 3H, OCH_3), 3.81 (s, 3H, OCH_3), 3.82-3.88 (m, 1H, H-5), 4.83 (dd, 1H, *J* = 11.0, 7.5 Hz, H-4), 4.98–5.02 (m, 2H, 9'-CH_2), 5.47–5.55 (m, 1H, H-8'), 6.75 (d, 1H, *J* = 9.0 Hz, ArH), 6.80 (d, 2H, *J* = 9.0 Hz, ArH), 6.85 (d, 2H, *J* = 8.5 Hz, ArH), 6.99 (d, 2H, *J* = 9.0 Hz, ArH), 7.27-7.35 (m, 3H, ArH), 8.02–8.04 (m, 2H, Ar-H), 8.46 (s, 1H, 1''-NH). ^{13}C NMR (125 MHz, $CDCl_3$): δ_C 34.74, 44.65, 54.52, 55.25, 55.29, 56.50, 57.42, 61.04, 66.16, 76.24, 108.34, 113.70, 114.04, 118.00, 124.01, 125.75, 127.32, 128.77, 129.85, 130.27, 130.54, 132.32, 133.77,

139.00, 143.10, 147.58, 158.59, 160.41, 177.65, 197.95. Anal. calcd for $C_{34}H_{34}N_4O_6$: C, 68.67; H, 5.76; N, 9.42 %; found: C, 68.51; H, 5.63; N, 9.55 %.

2.1.3. Spiro[2.3″]5″-fluorooxindole-spiro[3.3′]-1′-allyl-5′-(4-methoxyphenylmethylidene)-tetrahydro-4′(1H)-pyridinone-4-(4-methoxyphenyl)-pyrrolidine (6b)

Mp:189-190 °C; ^{1}H NMR (500 MHz, $CDCl_3$): δ_H 1.81 (d, 1H, *J* = 13.0 Hz, 2'-CH_2), 2.14, (s, 3H, N-CH_3), 2.70 (dd, 1H, *J* = 13.5, 7.5 Hz, 7'-CH_2), 2.88 (dd, 1H, *J* = 14.5, 2.5 Hz, 6'-CH_2), 3.06 (dd, 1H, *J* = 13.5, 5.0 Hz, 7'-CH_2), 3.28 (dd, 1H, *J* = 12.5, 1.5 Hz, 2'-CH_2), 3.30-3.34 (m, 1H, 5-CH_2), 3.46 (d, 1H, *J* = 14.5 Hz, 6'-CH_2), 3.79 (s, 3H, OCH_3), 3.80 (s, 3H, OCH_3), 3.86-3.90 (m, 1H, H-5), 4.75 (dd, 1H, *J* = 11.0, 7.5 Hz, H-4), 4.97–5.00 (m, 2H, 9'-CH_2), 5.51–5.57 (m, 1H, H-8'), 6.54-6.57 (m, 1H, ArH), 6.76 (td, 1H, *J* = 9.0, 2.5 Hz, ArH), 6.82-6.85 (m, 4H, ArH), 6.88 (dd, 1H, *J* = 8.5, 2.5 Hz, ArH), 7.09 (d, 2H, *J* = 8.5 Hz, ArH), 7.28 (s, 1H, ArH), 7.33 (d, 2H, *J* = 8.5 Hz, ArH), 7.91 (s, 1H, 1''-NH). ^{13}C NMR (125 MHz, $CDCl_3$): δ_C 34.71, 45.01, 54.36, 55.24, 55.27, 56.45, 57.26, 60.97, 65.93, 76.49, 108.90, 113.60, 113.88, 114.97, 115.64, 117.54, 127.74, 129.55, 130.25, 130.54, 131.00, 132.17, 134.19, 137.75, 138.33, 158.47, 158.90, 160.18, 177.63, 198.61. Anal. calcd for $C_{34}H_{34}FN_3O_4$: C, 71.94; H, 6.04; N, 7.40 %; found: C, 71.75; H, 6.27; N, 7.51 %.

2.2. X-ray details

The compounds **6(a,b)** were obtained as single crystals by slow evaporation from ethylacetate solution of the pure compound at room temperature. Data were collected on a Bruker APEX-II D8 Venture area diffractometer, equipped with graphite monochromatic Mo Kα radiation, λ = 0.71073 Å. Cell refinement and data reduction were carried out by Bruker SAINT. SHELXT [25,26] was used to solve structure. The final refinement was carried out by full-matrix least-squares techniques with anisotropic thermal data for nonhydrogen atoms on *F*.

2.3. Hirshfeld surface analysis

The topology analyses were performed using Crystal Explorer 17.5 program [27].

2.4. Computational methods

All DFT calculations were performed using Gaussian 09 software package [28] using B3LYP/6-31G(d,p) method. Natural bond orbital (NBO) analysis was performed using NBO 3.1 program as implemented in the Gaussian 09W package [29].

Journal Pre-proof

3. Results and Discussion

3.1. Synthesis

In our initial endeavor, the pre-requisite bismethoxyphenylmethylidene-piperidone **2** was synthesized following the literature reported method [30]. The dipolarophiles, N-allyl-bismethoxyphenylmethylidene-piperidone **3** required for the present study was prepared from the reaction of **2** with allyl chloride [31] while the other component, the azomethine ylide is generated *in situ* from the reaction of isatin (**4**) and sarcosine (**5**). With the functionalized dipolarophiles **3** in hand, we attempted the cycloaddition of **3** with azomethineylide generated *in situ* from 4-nitroisatin **4a** and sarcosine. Initially, we performed the cycloaddition reaction in a conventional solvent, methanol. The reaction of N-substituted dipolarophiles 3, **4a** and **5** in 10 mL of methanol was refluxed with constant stirring. The reaction progression and completion were evidenced through TLC analysis. After 1 h of reaction time, formation of the sole product, the spirooxindole-pyrrolidine **6a** was extracted in good yield (86%) from the reaction mixture. Towards our endeavor in the synthesis of heterocyclic hybrids employing green protocols, we planned to perform the same reaction in an ionic liquid. The same reaction was performed in [bmim]Br at 100 ^{o}C (Scheme 1). TLC analysis of the reaction mixture revealed completion of the reaction in about 30 minutes displaying the formation of the sole reaction product. The reaction mixture was then extracted with ethyl acetate and further purified by column chromatography. It is pertinent to note that the reaction in [bmim]Br afforded relatively a better yield (90%) of the spiropyrrolidine heterocyclic hybrid **6a** over the conventional heating employing methanol (86%). The ionic liquid [bmim]Br used in the above reaction was recycled in its pure form as done by us earlier [11]. The recycled [bmim]Br was then used for the other reaction employing 4-fluoroisatin **4b**. This reaction also afforded the spiropyrrolidine **6b** in an excellent yield (92%) in same reaction time revealing that the original properties of the ionic liquid has been maintained even after its recyclization. The molecular structure of spirooxindole-pyrrolidines **6(a,b)** was derived through ^{1}H and ^{13}C NMR spectroscopic studies (vide supporting data) and elemental analysis data. The presence of diverse functionalities makes these molecules more attractive for generating different supramolecular scaffolds.

Journal Pre-proof

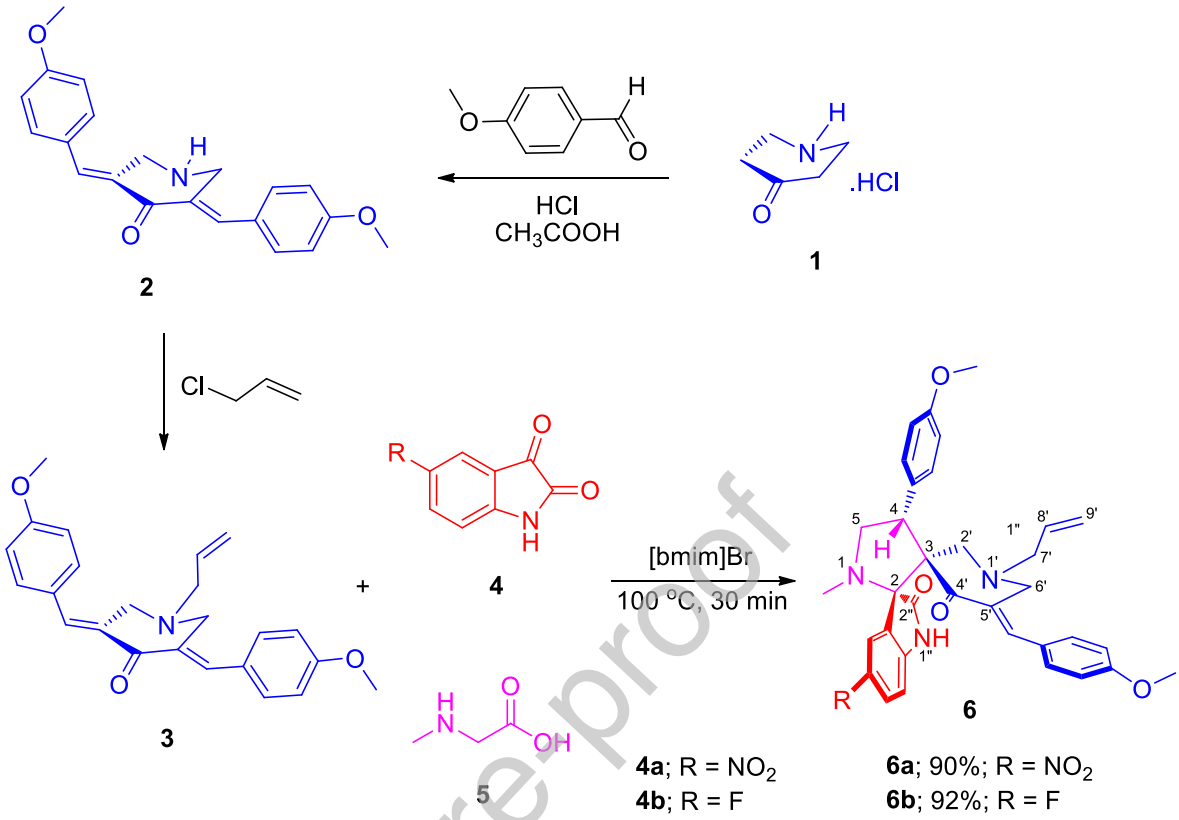

Scheme 1 Synthesis of spirooxindole-pyrrolidine hybrids **6(a,b)**

A comprehensible mechanism for the construction of heterocyclic hybrids **6** is displayed in scheme 2. The electron-deficient hydrogen atom of $[bmim]^+$ possibly will form hydrogen bond with one of the carbonyl group of 4-nitro or 4-fluoroisatin enabling the nucleophilic attack of the amino group of sarcosine on isatin. The intermediate **7** formed by dehydration affords the cyclic intermediate **8**. Compound **8** on decarboxylation provides the azomethine ylide. At the same time, the formation of hydrogen bond between the hydrogen atom of ionic liquid and the carbonyl group of dipolarophile **3** may further enhance rate of the reaction to afford **6**.

Journal Pre-proof

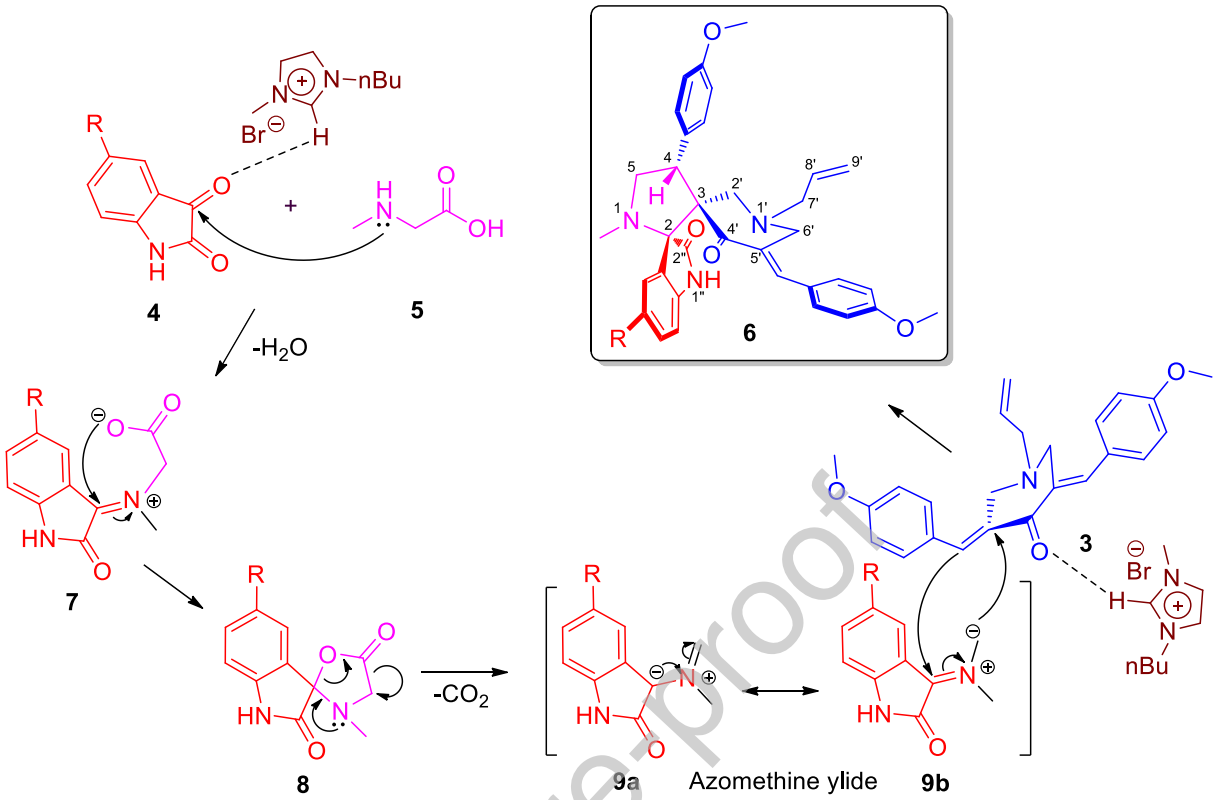

Scheme 2 Proposed mechanism for the formation of spirooxindole-pyrrolidine heterocyclic hybrids **6**

3.2. X-ray crystallographic studies

X-ray crystallographic study of a single crystals of **6a** [32] and **6b** [33] (Fig. 1) confirms the structures inferred from NMR spectroscopic studies.

6a

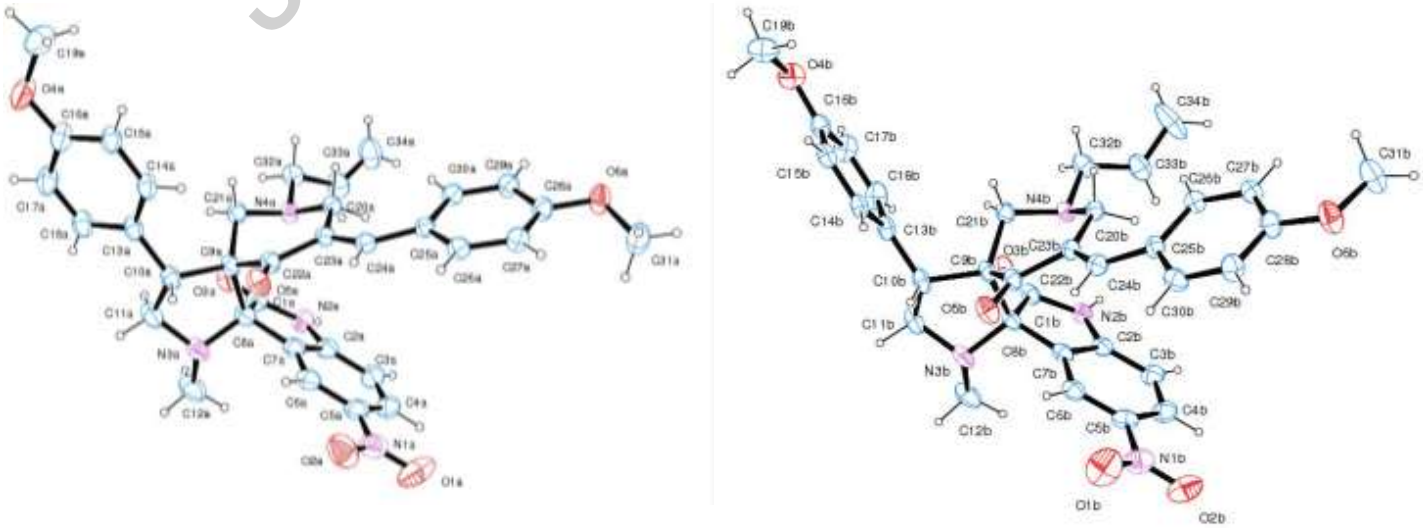

Journal Pre-proof

6b

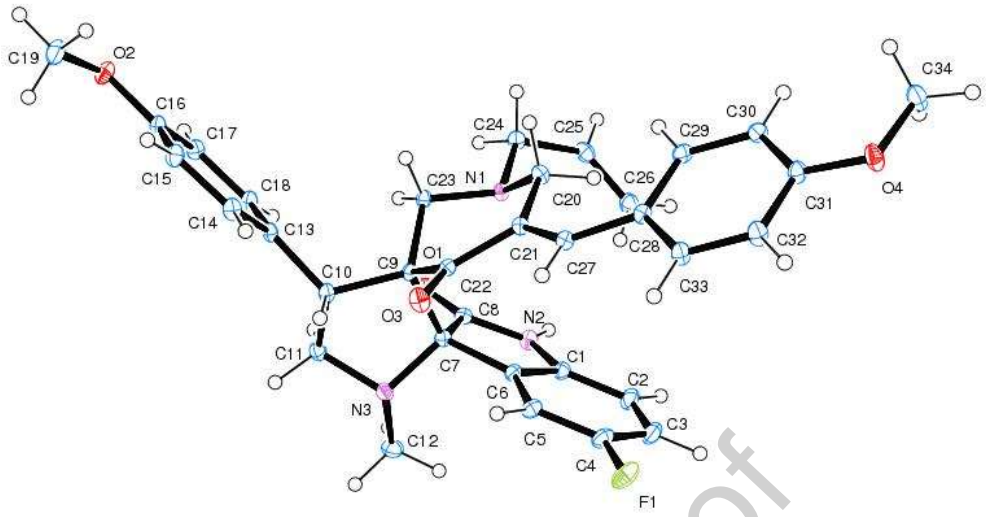

Fig. 1 ORTEP diagrams of Molecule A (left) and B (right) of **6a** and **6b** with displacement ellipsoids plotted at 20% and 30% probability level respectively.

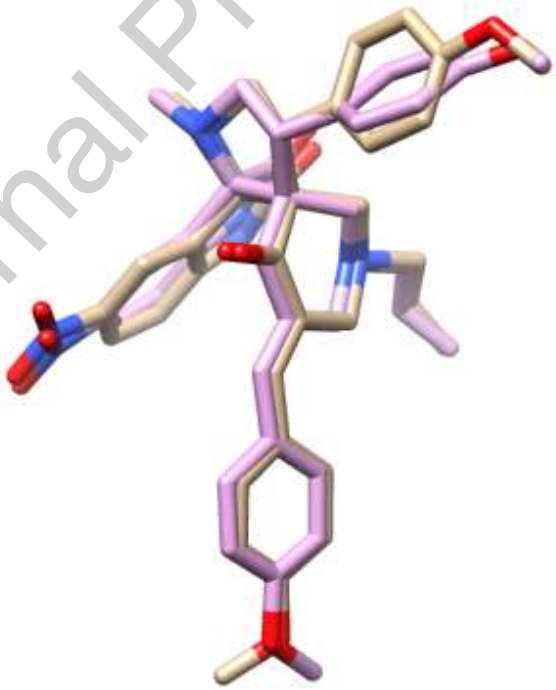

Fig. 2 Superimposed structures of the two molecules in the asymmetric unit of the compound **6a**

Journal Pre-proof

A view of the hydrogen bonding pattern of compounds **6a** and **6b** are shown in **Fig.3.**

6a

6b

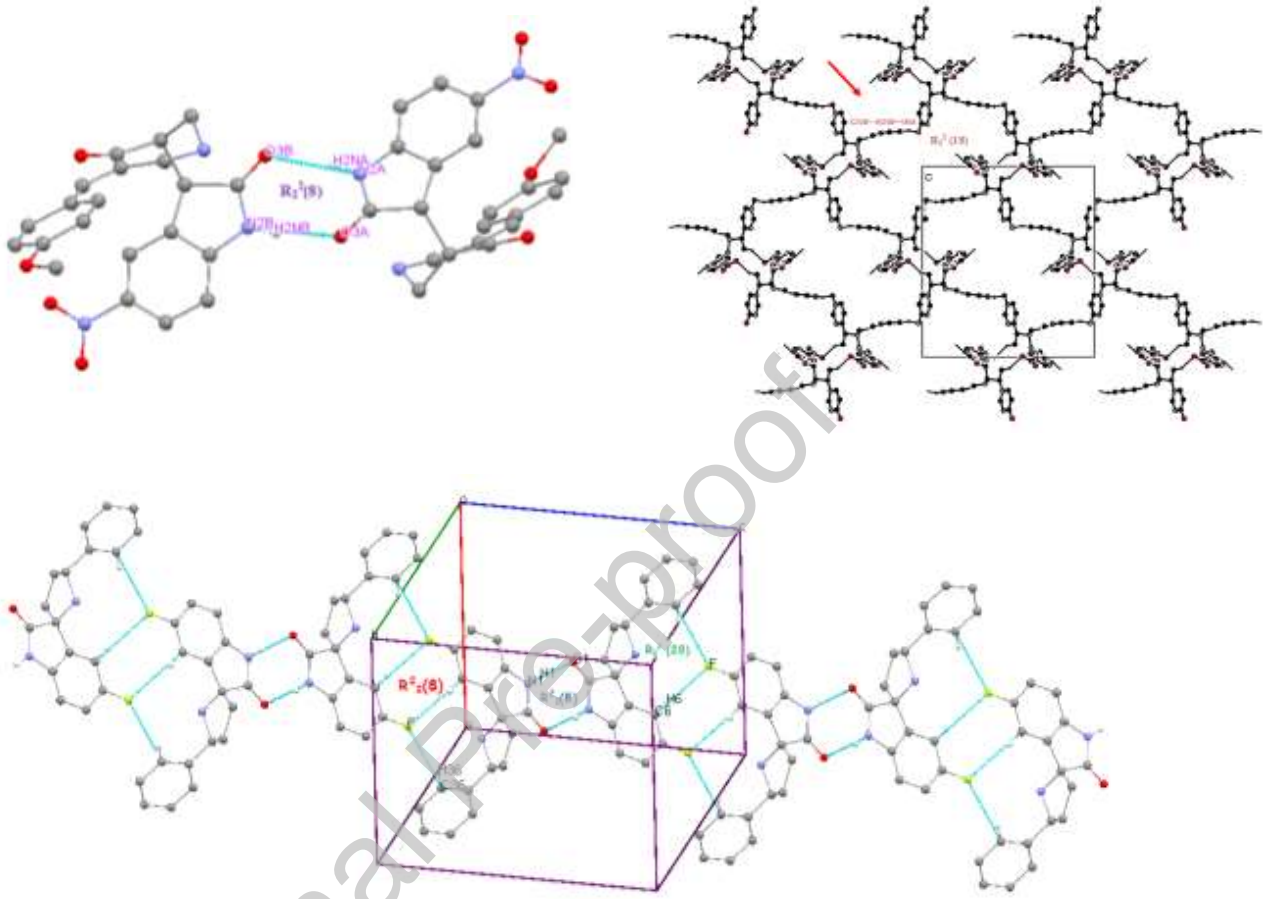

Fig. 3 View of the intermolecular hydrogen bonding pattern of compounds **6a** and **6b.** The non-interacting atoms are removed for clarity.

The crystallographic data, conditions used for the intensity data collection and some features of the structure refinements are listed in Table 1. The geometrical parameters like bond length, bond angles and dihedral angles are provided in the Tables S1 and S2 for the molecules **6a** and **6b**. The selected geometric parameters like bond lengths from X-ray data and DFT calculations are listed in Table S1 & S2 and Table S3 for the compounds **6a** and **6b** respectively. The unit cell of the crystal structure of compound **6a** contains two independent molecules with different conformation, which is evidenced by the methoxy group in molecule A & B have different orientations (Fig. 1). The superimposition of the independent monomers yielded RMSD

Journal Pre-proof

of 1.016 Å (Fig. 2). In both the molecules, the bond length and bond angles show normal values and agree with each other [34] except for the bonds at spiro junction.

The sum of angles at atoms N1*A*, N1*B* in molecules A and B of **6a**, N1 of compound **6b** of the pyrrolidine rings [337.06 (2)°, 339.55 (2) and 336.57 (2)° respectively] are in accordance with sp^3 -hybridization [35] while the sums of angles at atoms N2*A*, N2*B* in molecules A and B of **6a**, N2 of compound **6b** of the indolin-2-one moiety are in agreement with sp^2-hybridization [359.07 (2)°, 359.79 (2)°, and 360 (2)° respectively] [36]. In all the compounds the bond lengths among the indolin-2-one moiety match those in comparable structures but the C—C and C—N bonds within the pyrrolidine ring are shorter. The six-membered piperidone rings in compounds (Figs. 1-2) adopt the half-chair conformation, with deviations of atoms C21*A* and C23*A* from the least-squares plane defined by atoms C20*A*/C22*A*/C9*A*/N3*A* of -0.7724(4) and 0.1454 (5) Å in molecule A of **6a**, 0.7510 (4) and 0.1160 (4) in molecule B of **6a**, 0.7284 (1) and 0.2197 (1) Å in **6b** and 0.7179 (2) and 0.3153 (2) Å, respectively. The significant change in this variation is due to steric hindrance of the different substituents present at the C9 and C23 positions of the piperidine ring. The olefinic double bond in both the structures has an E conformation and the pyrrolidine ring takes up the envelope conformation. The two spiro junctions at atoms C8 and C9 in the molecule link a 2-oxindole ring, a pyrrolidine ring and a piperidone ring.

The pyrrolidine ring (N2/C8/C9/C10/C11) is in an envelope conformation, which is same as in the previously reported similar structures, it is the C atom of the CH_2 group of the pyrrolidine which forms the flap of the envelope or the N atom [37,38]. The puckering parameters and the smallest displacement asymmetry parameters are q_2 = 1.6228 (6) Å, φ = 59.32 (1) ° and ΔS (C21*A*)= 0.1590 (4) Å for piperidone ring and q_2 = 0.4341 (1) Å, φ= 147.57 (1) ° and ΔS (C11*A*) = 0.0612 (7) Å for pyrrolidine, molecule A of **6a**, q_2 = 1.5529 (1) Å, φ= 58.26 (2) ° and ΔS (C21*B*)= 0840 (7) Å for piperidone ring and q_2 = 0.4173 (9) Å, φ = 162.52 (9) and ΔS (N2*B*) = 0.1027 (9) Å for pyrrolidine , molecule B of **6a,** q_2 = 2.2738 (3) Å, φ= 88.07 (5) ° and ΔS (C20)= 0. 2932 (1) Å for piperidone ring and q_2 0.5461 (2) Å, φ= -9.37 (9) ° and ΔS (C8) = 0.0612 (7) Å for pyrrolidine of **6b**. The geometric plane that contains all the atoms in the phenyl rings in both the structures are not same with the mean plane of the piperidone ring; the torsion angle C23*A* —C24*A*—C25*A*—C26*A* is 6.43 (3)Å in molecule A of **6a**, C23*B*—C24*B*—C25*B*—C26*B* is 8.15 (2) Å in molecule B of **6a**, C23—C24—C25—C26 is -12.50 (3)Å in **6b**. This lack of coplanarity is caused by non-bonded interactions between one of the ortho H atoms

in the aryl ring and the equatorial H atoms at the 2-position of the piperidone ring (H26*A*/H20*A* or H20*B*) in molecule A of **6a**, (H26*B*/H20*C* or H20*D*) in molecule B of **6a**, (H26/H20*A*) in **6b**. Steric repulsions are reduced by the expansion of the C23*A*—C24*A*—C25*A* angle [133.98° in molecule A of **6a**], C23*B*—C24*B*—C25*B* angle [132.47° in molecule B of **6a**], C23—C24—C25 angle [132.90° in **6b** respectively]. The C8*A*—N2*A*, C11*A* -N2*A* bond length 1.477 (3) Å, 1.447 (2)Å in molecule A of **6a**, C8*B*—N2*B*, C11*B* -N2*B* bond length 1.462 (2) Å,1.446 (2) Å in molecule B of **6a**, C8—N2 , C11 - N2 bond length 1.475 (3) Å, 1.456 (2) Å in **6b**, and these values are comparable with the Csp^2—Nsp^2 distances found in similar structures [39].

The exocyclic angles around C28*A*, C16*A* in molecule A of I, C28*B*, C16*B* in molecule B of **6a** and C28 in compound **6b** show considerable asymmetry, with O4*A*— C27*A*—C28*A*, O2*A* — C16*A*—C17*A* in molecule A of **6a**, O4*B*—C27*B*—C28*B*, O2*B*- C16*B*—C17*B* in molecule B of **6a**, O4—C27—C28 in compounds **6b** being wider than O4*A*—C28*A*—C29*A*, O2*A*— C16*A*—C15*A* in molecule A of **6a**, O4*B*—C28*B*—C29*B*, O2*B*—C16*B*—C15*B* in molecule B of **6a**, and O4—C28—C29 in **6b** respectively (values listed in Table S1 and S2). This difference is due to the steric repulsion between the benzyl rings and its attached methyl groups of the methoxy phenyl rings. The torsion angles C31*A*—O4*A*—C28*A*—C29*A*, C31*A*—O4*A*—C27*A*—C28*A* and C19*A*—O2*A*—C16*A*—C17*A*, C19*A*—O2*A*—C16*A*—C15*A* in molecule A of **6a**, C31*B*—O4*B*—C28*B*—C29*B*, C31*B*—O4*B*—C27*B*—C28*B* and C19*B* —O2*B*—C16*B*—C17*B*, C19*B*—O2*B*—C16*B*—C15*B* in molecule B of **6a**, C31—O4—C28—C29, C31—O4—C27— C28 and C19—O2—C16—C17 in compounds **6b** indicate that the methoxy group does not deviate significantly from coplanarity with its benzene ring (values listed in Table S1 and S2). The benzene and pyrrole rings present in the indolin-2-one systems are individually planar and make dihedral angles of 4.81 (6)°, 3.97 (6), 2.40 (1)° in molecule A, B of **6a** and **6b**, respectively while the deviation of the atoms O1A, O1B and O1 in molecule A, B of **6a**, **6b** from the pyrrole ring of the indolin-2-one systems by 0.1360 (2) Å, -0.0949 (3) Å, and 0.0143 (9) Å respectively is because these O atoms are involved in different interactions (Tables 2 and 3). The indolin-2-one moiety stands nearly perpendicular with the respective to the pyrrolidine rings which is evidenced from the dihedral angles [85.39 (2°), 85.95 (1)° and 84.03 (4)°].

The geometry of the oxindole part of the molecules is fundamentally very similar for both the structures, and contrasts intently with oxindole fragments found in the pursuit of the Cambridge Structural Database (CSD, Version 5.30 with November 2008 and February 2009

updates; Allen, 2002). Also, in the two structures the atom C8 is sp^3 hybridized, displays remarkably longer C7*A*—C8*A*, C1*A*—C8*A*, C7*B*—C8*B*, C1*B*—C8*B*, C7—C8 bond lengths in molecule A, B of **6a** and **6b**, respectively which is due to the effect of spiro attachment at atom C8. The oxindole part of all the structures is exceptionally planar, while the whole molecule does not commonly digress a long way from planarity and this by all accounts identified with the formation of intramolecular interactions between groups in the oxindole and substituent segments of the molecules. The structures are also affected by the formation of intermolecular hydrogen bonds involving the oxindole N—H and C=O units, which leads to the formation of molecular dimers in every case. The hydrogen-bonding motif prompting to the formation of the molecular dimers can be portrayed as an R_2^2 (8) ring. The hydrogen-bonded networks of **6a** and **6b** are formed by a combination of N—H···O and C—H···X (where X= O in **6a** and **6b**) hydrogen-bonded supramolecular motifs.

In **6a**, an C29*A*—H29*A*···O2*A* $^{(i)}$ [symmetry code: (i) 2-x, 1/2+y, 1/2-z] (Table 2) hydrogen bonded C (14) motif [40] links molecules into a linear chain parallel to the [001] direction. The C(14) motif along the b axes, is the fundamental linking units in the formation of a supramolecular two-dimensional corrugated sheet parallel to the (100) plane characterized by R_2^2(18) and R_2^2 (18) motifs [40] (Fig.3) formed due to C11*A*—H11*A*···O6*A*$^{(ii)}$ and C20*B*— H20*D*···O5*A*$^{(iii)}$ [symmetry codes: (ii) 2-x, -y,1-z, (iii) x, 1/2-y, -1/2+z]. In addition, the C19*B*—H19*D*···O1*A*$^{(iv)}$ [symmetry code: (iv) -1+x, y, z] (Table 2) hydrogen bonded C(13) [40] chain and its inversion-related pair are connected through N— H···O bond dimers between the oxindole rings (Fig. 3).

In **6b**, N— H···O$^{(i)}$[symmetry code: (i) 1-x, 1-y, 1-z] (Table 2) hydrogen bonded R_2^2(18) motif [40] links molecules along b axes. Each such chain is linked to its adjacent parallel pairs through an C36— H36···F$^{(ii)}$ and C6— H6···F$^{(ii)}$ [symmetry code: (ii) 1-x,1-y, -z] hydrogen bonded characterized by R_2^2(20) and R_2^2 (8) ring motif [40] respectively, leading to the formation of a two-dimensional supramolecular sheet parallel to the (100) plane (Fig. 3).

The absence of O—H···O hydrogen bonds in the molecular interaction pattern, in spite of there being sufficient scope for them due to the presence of twelve O atoms in the compound **6a** and four O atoms in compound **6b** respectively, is prominent in the regard of the prediction of intermolecular interaction patterns. In addition, there are weak π…π stacking interactions as indicated by the relatively long C28···C29 (3.540(2) Å; symmetry code: 1-x,2-y,-z) and C28···C30 (3.595(2) Å; symmetry code: 1-x,2-y,-z) distances for **6b**. The shortest π…π contact

in **6a** is 3.362 Å (C4*A*···C4*B*; symmetry code: 1+x,-1/2-y,-1/2+z). It was believed that the π-π stacking interactions could exist at large C···C distances up to 7 Å [41].

Table 1 The crystal and experimental data of compound **6a** and **6b**

Crystal data	**6a**	**6b**
Chemical formula	$C_{34}H_{34}N_4O_6$	$C_{34}H_{34}FN_3O_4$
*M*r	594.65	567.64
Crystal system, space group	Monoclinic, $P2_1/c$	Triclinic, *P-1*
Temperature (K)	293	100
a, *b*, *c* (Å)	12.3598 (9), 21.1459 (16), 24.9180 (15)	11.4244 (3), 11.8388 (3), 11.9418(6)
α, β, γ(°)	90, 109.686 (3), 90	99.649 (2), 92.791 (2), 116.274 (1)
V (Å^3)	6131.9 (7)	1413.93 (9)
Z	8	2
Radiation type	Mo *K*α	Mo *K*α
μ (mm^{-1})	0.09	0.09
Crystal size (mm)	0.58 × 0.20 × 0.19	0.33 × 0.27 × 0.16
Data collection		
Diffractometer	Bruker Kappa APEXII	Bruker Kappa APEXII
Absorption correction	Multi-scan *SADABS*; Sheldrick 1996	Multi-scan *SADABS*; Sheldrick 1996
T_{min}, T_{max}	0.950, 0.983	0.971, 0.986
No. of measured, independent and observed [I> 2σ(I)] reflections	58820, 14048, 7210	29178, 6478, 4961
R_{int}	0.040	0.051
Refinement		
R[F^2> 2σ(F^2)], wR(F^2), S	0.075, 0.277, 1.01	0.045, 0.126, 1.10
No. of reflections	14048	6478
No. of parameters	799	383
No. of restraints	0	0
$\Delta\rho_{max}$, $\Delta\rho_{min}$ (e Å^{-3})	0.59, −0.29	0.32, −0.19
CCDC number	**1452069**	**1572706**

Journal Pre-proof

Table 2 Hydrogen-bonding parameters (Å, °) of compound **6a and 6b**

D—H···*A*	*D*—H	H···*A*	*D*···*A*	*D*—H···*A*
C6*B*—H6*BA*···O3*B*	0.93	2.60	3.209 (5)	124
C10*B*—H10*B*···O3*B*	0.98	2.28	2.795 (4)	112
C11*B*—H11*D*···O1*B*	0.97	2.57	3.156 (4)	119
C19*B*—H19*D*···O1*A*	0.96	2.43	3.248 (6)	143
C21*B*—H21*C*···O1*B*	0.97	2.36	2.936 (4)	118
N1*A*—H1*NA*···O1*B*^{i}	0.86	2.03	2.855 (4)	160
N1*B*—H1*NB*···O1*A*^{ii}	0.88	2.01	2.895 (4)	173
C11*A*—H11*A*···O6*A*^{iii}	0.97	2.49	3.296 (5)	141
C19*B*—H19*E*···O6*A*^{iv}	0.96	2.41	3.023 (7)	121
C20*B*—H20*D*···O5*A*^{v}	0.97	2.56	3.495 (6)	161
C29*A*—H29*A*···O2*A*^{vi}	0.93	2.59	3.333 (5)	138

Symmetry codes: (i) *x*, −*y*+1/2, *z*+1/2; (ii) *x*, −*y*+1/2, *z*−1/2; (iii) −*x*, −*y*, −*z*+1; (iv) *x*+1, *y*, *z*; (v) *x*+1, −*y*+1/2, *z*−1/2; (vi) −*x*, *y*+1/2, −*z*+1/2.

D—H···*A*	*D*—H	H···*A*	*D*···*A*	*D*—H···*A*
C6—H6···O3	0.93	2.57	3.1710 (19)	123
C10—H10···O3	0.98	2.25	2.7804 (19)	113
C21—H21*B*···O1	0.97	2.37	2.9473 (19)	117
N1—H1···O1^{i}	0.86	2.07	2.9088 (17)	167
C6—H6···F^{ii}	0.97	2.60	3.2048 (19)	121
C36—H36···F^{ii}	0.97	2.55	3.345 (2)	139

Journal Pre-proof

Symmetry codes: (i) −*x*+1, −*y*+1, −*z*+1; (ii) −*x*+1, −*y*+1, −*z*

3.3. Hirshfeld Analysis

Analysis of molecular packing for **6a** and **6b** with the aid of Hirshfeld calculations are presented in Figs. S5 and S6 (Supplementary data), respectively. The decomposed fingerprint plot of each intermolecular contact shed the light on its percentage contribution in the molecular packing. Since, the asymmetric unit in the crystal structure of **6a** comprised two molecular units so; Fig. 4 gives the percentages of all intermolecular contacts for both molecular units in the crystal of **6a**. Summary of the most important contacts are listed in table 3 while the corresponding fingerprint plots are shown in Fig. 5.

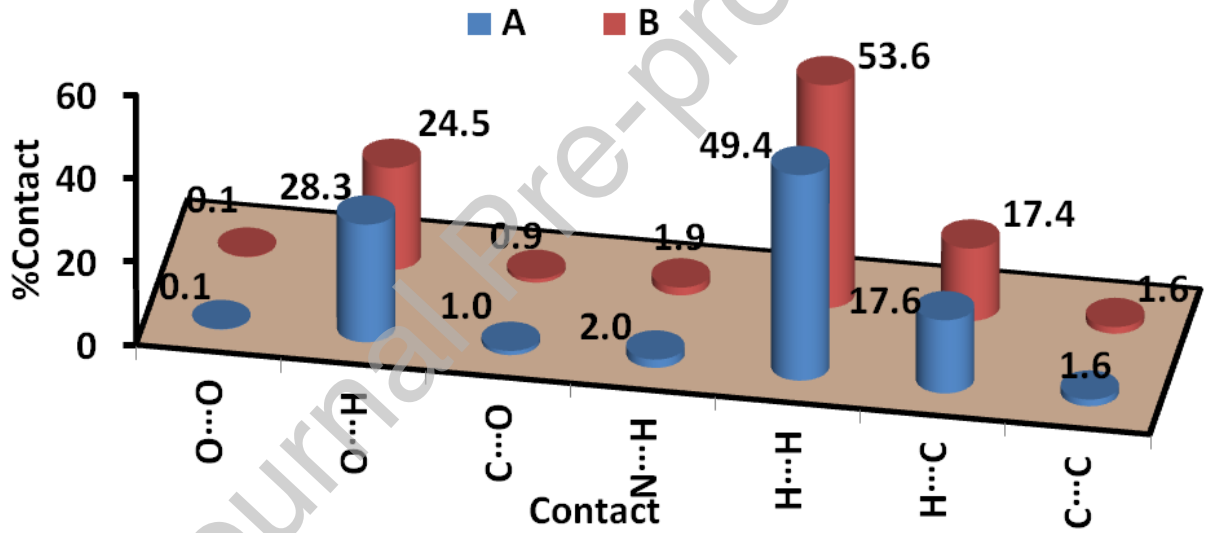

Fig. 4 The contributions of each intermolecular contact in the molecular packing of **6a**. For definition of **A** and **B**, refer to **Fig. S5** (vide supplementary data).

Journal Pre-proof

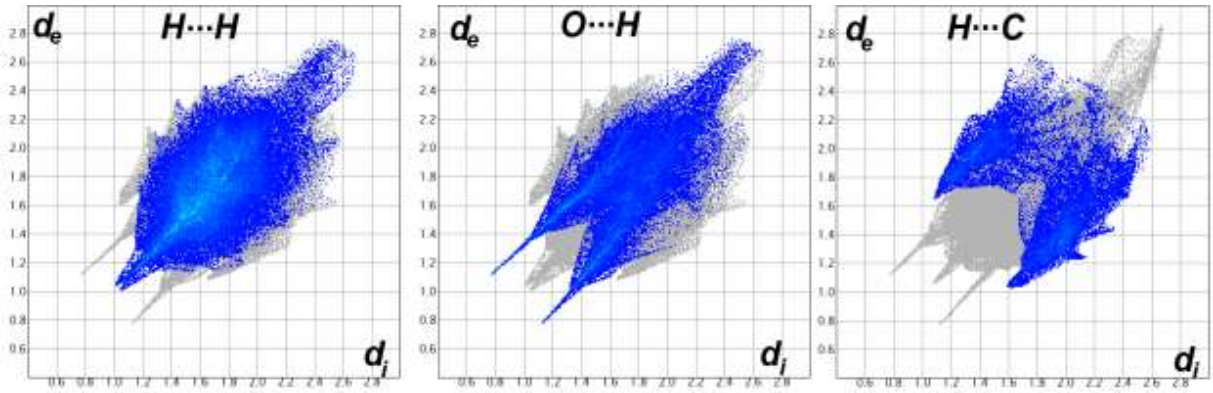

Fig. 5 Decomposed fingerprint plots of the important contacts in **6a**.

Table 3 The shortest H···H, O···H and H···C contacts in **6a**.

Contact	Distance	Contact	Distance
O1*A*···H20*D*	2.456	O2*A*···H11*A*	2.404
O1*A*···H33*B*	2.571	O4*A*···H29*A*	2.476
O2*A*···H19*E*	2.349	H26*A*···C15*B*	2.729
O3*A*···H19*D*	2.336	H26*A*···C16*B*	2.642
O4*B*···H21*A*	2.527	H4*BA*···C25*A*	2.741
O1*B*···H19*C*	2.581	H10*A*···H31*F*	2.140
O3*A*···H2*NB*	1.891	H19*C*···H34*B*	2.053
O3*B*···H2*NA*	1.893		

It is clear that, the molecular packing in the crystal structure of **6a** is dominated by H···H, O···H and H···C(π) contacts. The other intermolecular contacts are less dominant and considered weaker compared to the significant O···H, H···C(π) and H···H interactions. These interactions appeared as red regions in the d_{norm} map indicating their significance (**Fig. 6**). The O···H contacts ranges from 1.891 Å (O3*A*···H2*NB*) to 2.581 Å (O1*B*···H19*C*) while the C-H···π interactions ranging from 2.642 Å (H26*A*···C16*B*) to 2.741 Å (H4*BA*···C25*A*). On other hand, the H···H contacts are the most common. The shortest H···H interaction distances are 2.140 and 2.053 Å for H10*A*···H31*F* and H19*C*···H34*B*, respectively.

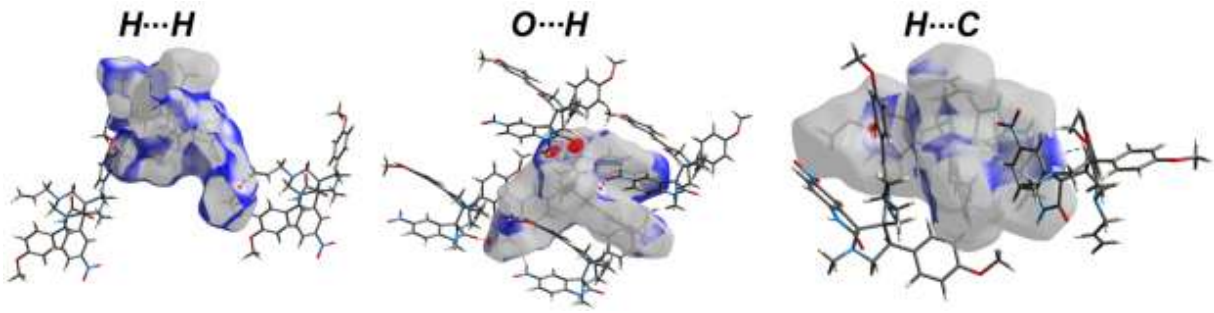

Fig. 6 Decomposed d_{norm} maps showing the most important H···H, O···H and H···C(π) interactions in **6a**. All appeared as red spots indicating significant interactions.

Also, the packing of **6b** is dominated by significant amount of H···H, O···H and H···C(π) contacts (**Fig. 7**) where the corresponding fingerprint plots for these interactions are presented in the upper part of **Fig. 8**. Similar to **6a**, the O···H interactions appeared as sharp spikes indicating that these contacts are strong in both compounds. In agreement with this observation, it appeared as intense red regions in the corresponding d_{norm} map (**Fig. 8**, lower part). The O···H contact distances ranging from 1.906 Å (O1···H1*N2*) to 2.472 Å (O4···H24*B*). Summary of the shortest contacts along with their interaction distances are listed in table 4. On other hand, the H···C (C-H···π) interactions appeared as less sharp spikes compared to the O···H contacts and hence considered weaker but with interaction distances shorter (2.704-2.705 Å) than those in **6a**. In contrast, the H···H interaction distances are shorter in the **6a** compared to **6b** (Table 4). Additionally, Hirshfeld calculations indicated some C···C contacts of 1.6 and 3.5% in **6a** and **6b** respectively. The C···C contacts are generally longer than the van der Waals radii sum of two carbons indicating weak π-π interactions.

Table 4 The H···H, O···H and H···C shortest contacts in **6b**

Contact	Distance	Contact	Distance
O3···H14*A*	2.212	H2*A*···C33	2.715
O4···H24*B*	2.472	H2*A*···C32	2.704
O1···H1*N2*	1.906	H10*A*···H34*B*	2.200

Journal Pre-proof

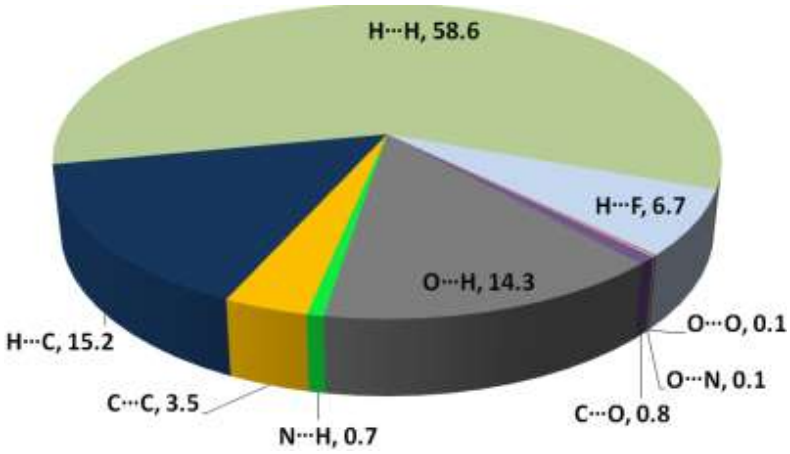

Fig. 7 Pie chart showing the intermolecular contacts and their percentages in **6b**.

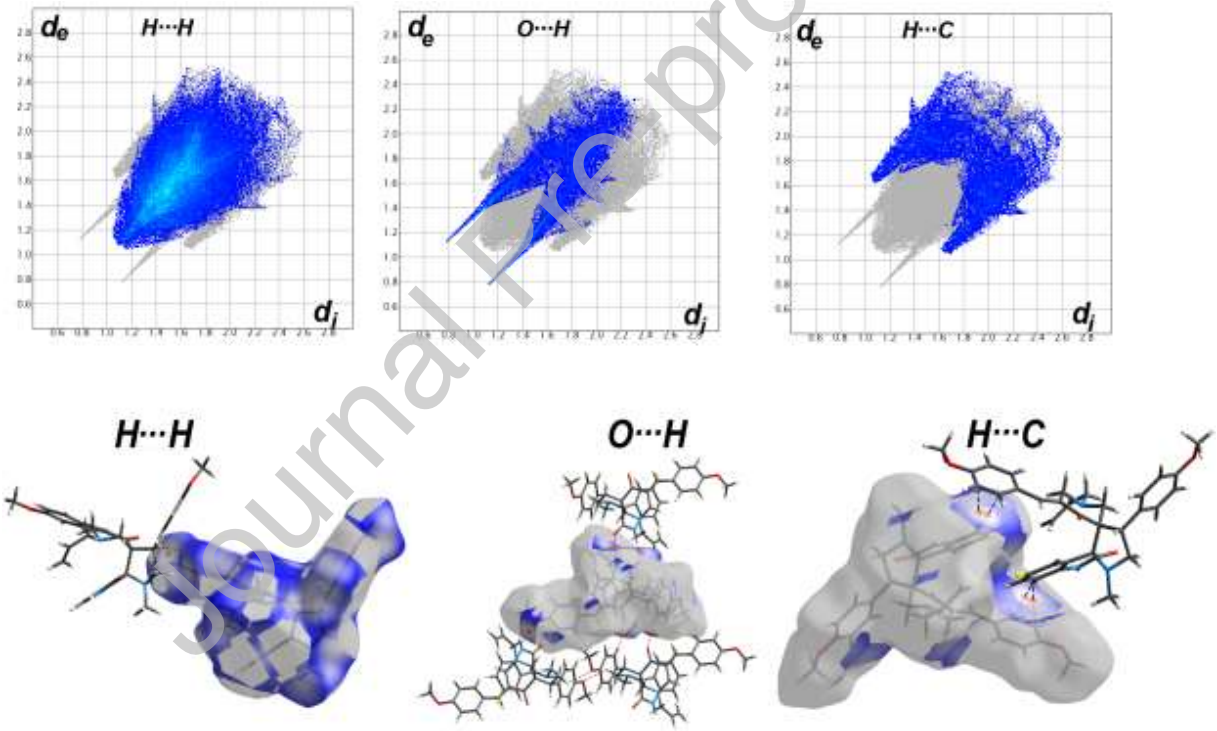

Fig. 8 Decomposed fingerprint plots (upper) and d_{norm} maps of the most important H···H, O···H and H···C interactions in **6b**.

3.4. DFT Studies

The optimized structural geometries of **6a** and **6b** are shown in Figs. S7 and S8 together with their matching with the corresponding experimental X-ray structures. It is clear that the calculated

structures are in good agreement with the experimental ones as indicated from the high correlation coefficients between the calculated and experimental bond distances (Fig. S9). The correlation coefficients for bond angles are 0.9824 and 0.9750, respectively. Complete list of bond distances and angles are given in table S3 (vide supplementary data). The partial charges at the different atomic sites are listed in table S4 (vide supplementary data). The studied molecules comprised many electronegative atoms such as nitrogen and oxygen which have the highest negative partial charges and most of carbon atoms as well. In contrast, all hydrogen atoms and carbon attached directly to either N or O sites are electropositive and the nitro group nitrogen atom as well. Presentation of the electron density mapped over molecular electrostatic potential (MEP) map is shown in Fig. 9. As a consequence of the presence of many polar sites in these compounds, the calculated dipole moment is predicted to be 6.415 and 5.552 Debye for **6a** and **6b**, respectively. The compound with nitro group (**6a**) is more polar than the one with fluoro-substituent (**6b**). In addition, the red regions in MEP which are related to the carbonyl oxygen atom represent the most probable sites as hydrogen bond acceptor while the blue or turquoise colored regions are related to N-H proton and some of the C-H protons which are the most candidates as hydrogen bond donor.

The HOMO and LUMO levels as well as their energies are important for studying the molecular reactivity of compounds (Fig. 9). The ionization potential (I), electron affinity (A), chemical potential (μ), hardness (η) as well as electrophilicity index (ω) are reactivity indices based on the HOMO and LUMO energies [42-48]. These parameters are calculated and the results are listed in Table 5. These descriptors are important to describe the ability of molecule towards charge transfer processes.

Table 5 The calculated reactivity indices of the studied compounds.

Parameter	**Equation**	**6a**	**6b**
HOMO		-5.6758	-5.4600
LUMO		-2.1935	-1.7704
I	$-E_{HOMO}$	5.6758	5.4600
A	$-E_{LUMO}$	2.1935	1.7704
η	(I-A)/2	3.4823	3.6896

Journal Pre-proof

μ	-(I+A)/2	-3.9347	-3.6152
x		3.9347	3.6152
ω	$\mu^2/2\eta$	2.2229	1.7711

The HOMO of both molecules has relatively close energies indicating their ability to donate electron is almost the same where **6b** has slightly higher ability to make electron donation than **6a**. In contrast, the LUMO of **6a** is lower than that for **6b**. Hence, **6a** which has the nitro group as strong electron withdrawing moiety has higher ability to accept electrons than **6b**. In agreement with these results, the electrophilicity (ω) of **6a** is higher than **6b**.

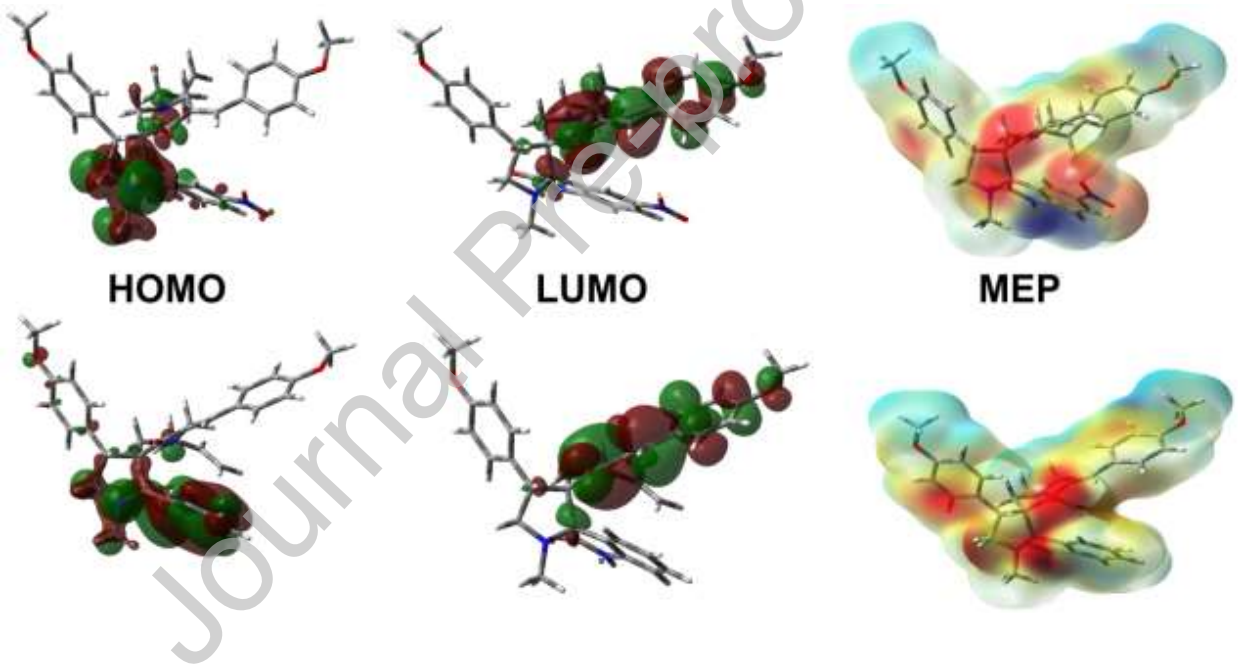

Journal Pre-proof

Fig. 9 The MEP maps of the **6a** (upper) and **6b** (lower). The color index from blue to turquoise to yellow to red in MEP indicated the more negative electron density.

3.5. NBO analysis

Analysis of the natural bond orbitals (NBO) included in the intramolecular charge transfer (IMCT) interactions sheds the light on the importance of electron delocalization processes in stabilizing the studied system [49,50]. The stabilization energy ($E^{(2)}$) of the different σ-σ*, π→π*, n→σ* and

n→π* charge transfer processes are listed in **Table S5** (Supplementary data). In general, the σ-σ* IMCT are weak with net stabilization energy of 16.0 and 26.0 kcal/mol for **6a** and **6b**, respectively. In contrast, there are many π→π* IMCT which stabilized the system. The net stabilization energy due to the π→π* IMCT processes are comparable in both compounds. Their net $E^{(2)}$ values are 388.75 and 395.27 kcal/mol, respectively. On other hand, the n→σ* are generally weaker than n→π* IMCT in both compounds. The net n→σ* IMCT stabilization energies are 168.78 and 124.58 kcal/mol for **6a** and **6b**, respectively. The corresponding values for the n→π* IMCT are 287.89 and 180.97 kcal/mol, respectively.

4. Conclusions

In the present study, structurally robust highly functionalized spirooxindole-pyrrolidine heterocyclic hybrids **6(a,b)** have been constructed stereoselectively through a [3+2] cycloaddition strategy in [bmim]Br. The ionic liquid, [bmim]Br played dual role both as the reaction medium and a catalyst thus accelerating the rate of the reaction affording the cycloadducts in excellent yields. The structure of these spiroheterocyclic hybrids was explicated by spectroscopic analysis and the stereochemistry has been established by single crystal X-ray crystallographic studies. The DFT calculated geometric parameters are in good agreement with the experimental data obtained from X-ray crystallography. Hirshfeld analysis revealed the importance of the O···H, H···H and H···C(π) interactions in the molecular packing of **6a** and **6b**. Their electronic properties and reactivity descriptors were computed using B3LYP/6-31G(d,p) method. NBO analyses revealed the importance of the different σ-σ*, π→π*, n→σ* and n→π* charge transfer processes in stabilizing the studied molecular systems. These interesting results obtained led us to explore and unearth structural properties more complex spiro heterocyclic analogues.

Acknowledgments

The authors extend their appreciation to the Deanship of Scientific Research at King Saud University for funding this work through research group no RG-1440-071.

Conflicts of Interest

The authors declare no conflict of interest.

Appendix A. Supplementary data

Supplementary data related to this article can be found at…

Journal Pre-proof

References

[1] J. Rodriguez, D. Bonne, (Eds.), Stereoselective multiple bond-forming transformations in organic synthesis. John Wiley and Sons, Hoboken, New Jersey, 2015.

[2] A. Padwa, (Ed.), 1,3-Dipolar Cycloaddition Chemistry, Vols. 1 and 2, Wiley, New York, NY, 1984.

[3] W.H. Pearson, in: A.U. Rahman (Ed.), Studies in Natural Product Chemistry, Vol. 1, Elsevier, Amsterdam, 1998, p. 323.

[4] F. Fache, E. Schulz, M.L. Tommasino, M. Lemaire. Nitrogen-containing ligands for asymmetric homogeneous and heterogeneous catalysis, Chem. Rev. 100 (2000) 2159-2232.

[5] P.I. Dalko, L. Moisan. In the golden age of organocatalysis, Angew. Chem. Int. Ed. 43 (2004) 5138-5175.

[6] G.S. Singh, Z.Y. Desta. Isatins As Privileged Molecules in Design and Synthesis of Spiro-Fused Cyclic Frameworks, Chem. Rev. 112 (2012) 6104-6155.

[7] A. Jossang, P. Jossang, H.A. Hadi, T. Sevenet, B. Bodo. Horsfiline, an oxindole alkaloid from Horsfieldia superba, J. Org. Chem. 56 (1991) 6527-6530.

[8] N. Anderton, P.A. Cockrum, S.M. Colegate, J.A. Edgar, K. Flower, I. Vit, R.I. Willing. Oxindoles from Phalaris coerulescens, Phytochemistry 48 (1998) 437-439.

[9] C. Pellegrin, M. Weber, H.eJ. Borschberg, Total synthesisof (+)-elacomine and (-)-isoelacomine, two hitherto unnamedoxindole alkaloids from Elueagnus cornrnutata, Helv. Chim. Acta 79 (1996) 151-168.

[10] W. Bao, Z. Wang. An effective synthesis of bromoesters from aromatic aldehydes using tribromide ionic liquid based on l-prolinol as reagent and reaction medium under mild conditions, Green Chem. 8 (2006) 1028–1033.

[11] R.S. Kumar, A.I. Almansour, N. Arumugam, S.M. Soliman, R.R. Kumar, M. Altaf, H.A. Ghabbour, B.S. Krishnamoorthy. Stereoselective green synthesis and molecular structures of highly functionalized spirooxindole-pyrrolidine hybrids – A combined experimental and theoretical investigation, J. Mol. Struct. 1152 (2018) 266-275.

[12] R.S. Kumar, A.I. Almansour, N. Arumugam, M. Altaf, J.C. Menéndez, R.R. Kumar, H. Osman. A Sustainable Approach to the Stereoselective Synthesis of Diazaheptacyclic Cage Systems Based on a Multicomponent Strategy in an Ionic Liquid, Molecules 21 (2016) 165.

Journal Pre-proof

[13] R.S. Kumar, A.I. Almansour, N. Arumugam, J.C. Menéndez, H. Osman, R.R. Kumar. Dipolar Cycloaddition-Based Multicomponent Reactions in Ionic Liquids: A Green, Fully Stereoselective Synthesis of Novel Polycyclic Cage Systems with the Generation of Two New Azaheterocyclic Rings, Synthesis 47 (2015) 2721-2730.

[14] R.S. Kumar, A.I. Almansour, N. Arumugam, A. Basiri, Y. Kia, R.R. Kumar. Ionic Liquid-Promoted Synthesis and Cholinesterase Inhibitory Activity of Highly Functionalized Spiropyrrolidines, Aust. J. Chem., 68 (2015) 863–871.

[15] A.I. Almansour, N. Arumugam, R.S. Kumar, P.V. Subbarayan, A.A. Alshatwi, H.A. Ghabbour, Anti-cancer compound, *US patent* 9486444, 2016.

[16] R.V. Sumesh, M. Muthu, A.I. Almansour, R.S. Kumar, N. Arumugam, S. Athimoolam, E.A.J.Y. Prabha, R.R. Kumar. Multicomponent Dipolar Cycloaddition Strategy: Combinatorial Synthesis of Novel Spiro-Tethered Pyrazolo[3,4-b]quinoline Hybrid Heterocycles, ACS Comb. Sci. 18 (2016) 262-270.

[17] A.I. Almansour, R.S. Kumar, N. Arumugam, A. Basiri, Y. Kia, M.A. Ali, M. Farooq, V. Murugaiyah. A facile ionic liquid promoted synthesis, cholinesterase inhibitory activity and molecular modeling study of novel highly functionalized spiropyrrolidines, Molecules 20 (2015) 2296-2309.

[18] A.I. Almansour, R.S. Kumar, F. Beevi, A.N. Shirazi, H. Osman, R. Ismail, T.S. Choon, B. Sullivan, K. McCaffrey, A. Nahhas, K. Parang, M.A. Ali. Facile, regio- and diastereoselective synthesis of spiro-pyrrolidine and pyrrolizine derivatives and evaluation of their antiproliferative activities, Molecules 19 (2014) 10033-10055.

[19] A.I. Almansour, R.S. Kumar, N. Arumugam, A. Basiri, Y. Kia, M.A. Ali. An expedient synthesis, acetylcholinesterase inhibitory activity, and molecular modeling study of highly functionalized hexahydro-1,6-naphthyridines, BioMed Res. Int. Volume (2015) 9. Article ID 965987.

[20] R.S. Kumar, A.I. Almansour, N. Arumugam, R.R. Kumar. Substitution induced switch between Pictet-Spengler and Eschweiler-Clarke reactions: Selective synthesis of spiro acenaphthylene pyrrolo[1,2-b]-isoquinoline/pyrrolidine hybrids, Tetrahedron Lett. 61 (2020) 151606.

Journal Pre-proof

[21] A.I. Almansour, N. Arumugam, R. S. Kumar, D. Kotresha, T. Sai Manohar, S. Venketesh. Design, synthesis and cholinesterase inhibitory activity of novel spiropyrrolidine tethered imidazole heterocyclic hybrids, Bioorg. Med. Chem. Lett. 30 (2020) 126789.

[22] R.S. Kumar, A.I. Almansour, N. Arumugam, F. Mohammad, D. Kotresha, J. C. Menendez. Spirooxindole-pyrrolidine heterocyclic hybrids promotes apoptosis through activation of caspase-3, Bioorg. Med. Chem. 27 (2019) 2487-2498.

[23] M. Bolous, N. Arumugam, A.I. Almansour, R.S. Kumar, K. Maruoka, V.C. Antharam, S. Thangamani. Broad-spectrum antifungal activity of spirooxindolo-pyrrolidine tethered indole/imidazole hybrid heterocycles against fungal pathogens, Bioorg. Med. Chem. Lett. 29 (2019) 2059-2063.

[24] N. Arumugam, A.I. Almansour, R.S. Kumar, D.M. Al-thamili, G. Periyasami, V.S. Periasamy, J. Athinarayanan, A.A. Alshatwi, S.M. Mahalingam, J.C. Menéndez. Regio and stereoselective synthesis of anticancer spirooxindolopyrrolidine embedded piperidone heterocyclic hybrids derived from one-pot cascade protocol, Chemistry Central Journal, (2018) 12:95.

[25] G.M. Sheldrick, A short history of SHELX. Acta Crystallogr. A. 64 (2008) 112–122.

[26] G.M. Sheldrick, SHELXTL-PC (Version 5.1), Siemens Analytical Instruments, Inc., Madison, WI, 1997.

[27] M.J. Turner, J.J. McKinnon, S.K. Wolff, D.J. Grimwood, P.R. Spackman, D. Jayatilaka, M.A. Spackman, Crystal Explorer 17 (2017) University of Western Australia. http://hirshfeldsurface.net

[28] M.J. Frisch, G.W. Trucks, H.B. Schlegel, G.E. Scuseria, M.A. Robb, J.R. Cheeseman, G.Scalmani, V.Barone, B.Mennucci, G.A. Petersson, H.Nakatsuji, M. Caricato, X. Li, H.P. Hratchian, A.F. Izmaylov, J.Bloino, G.Zheng, J.L. Sonnenberg, M. Hada, M. Ehara, K. Toyota, R. Fukuda, J. Hasegawa, M. Ishida, T. Nakajima, Y. Honda, O. Kitao, H. Nakai, T. Vreven, J.A. Montgomery, Jr., J.E. Peralta, F. Ogliaro, M. Bearpark, J.J. Heyd, E. Brothers, K.N. Kudin, V.N. Staroverov, R. Kobayashi, J. Normand, K. Raghavachari, A. Rendell, J.C. Burant, S.S. Iyengar, J. Tomasi, M. Cossi, N. Rega, J.M. Millam, M. Klene, J.E. Knox, J.B. Cross, V. Bakken, C. Adamo, J. Jaramillo, R. Gomperts, R.E. Stratmann, O. Yazyev, A.J. Austin, R. Cammi, C. Pomelli, J.W. Ochterski, R.L. Martin, K. Morokuma, V.G. Zakrzewski, G.A. Voth, P. Salvador, J.J. Dannenberg, S. Dapprich, A.D. Daniels, O. Farkas, J.B. Foresman, J.V. Ortiz, J. Cioslowski, D.J. Fox, GAUSSIAN 09. Revision A02. Gaussian Inc., Wallingford CT, USA (2009). GaussView, Version 4.1, R. Dennington II, T. Keith, J. Millam, Semichem Inc., Shawnee Mission, KS, (2007).

Journal Pre-proof

[29] A.E. Reed, L.A. Curtiss, F. Weinhold, Intermolecular Interactions from a Natural Bond Orbital, Donor-Acceptor Viewpoint, Chem. Rev. 88 (1988) 899–926.

[30] J.R. Dimmock, M.P. Padmanilayam, R.N. Puthucode, A.J. Nazarali, N.L. Motaganahalli, G.A. Zello, J.W. Quail, E.O. Oloo, H.B. Kraatz, J.S. Prisciak, T.M. Allen, C.L. Santos, J. Balzarini, E. De Clercq, E.K. Manavathu, A conformational and structure-activity relationship study of cytotoxic 3,5-bis(arylidene)-4-piperidones and related N-acryloyl analogues, J. Med. Chem. 44 (2001) 586–593.

[31] R.S. Kumar, A.I. Almansour, N. Arumugam, S.M. Soliman, R.R. Kumar, H.A. Ghabbour, Highly functionalized dispiro oxindole-pyrrolo[1,2-c]thiazole-piperidone hybrid: Synthesis, characterization and theoretical investigations on the regiochemistry, J. Mol. Struct. 1121 (2016) 93-103.

[32] Crystallographic data (including structure factors) for the compound **6a** have been deposited with the Cambridge Crystallographic Data Centre as supplementary publication number CCDC 1452069. Copies of the data can be obtained, free of charge, on application to CCDC, 12 Union Road, Cambridge CB2 1EZ, UK [fax: +44 (0)1223 336033 or e-mail: deposit@ccdc.cam.ac.uk].

[33] Crystallographic data (including structure factors) for the compound **6b** have been deposited with the Cambridge Crystallographic Data Centre as supplementary publication number CCDC 1572706. Copies of the data can be obtained, free of charge, on application to CCDC, 12 Union Road, Cambridge CB2 1EZ, UK [fax: +44 (0)1223 336033 or e-mail: deposit@ccdc.cam.ac.uk].

[34] F.H. Allen, O. Kennard, D.G. Watson, L. Brammer, A.G. Orpen, R. Taylor, Tables of Bond Lengths determined by X-Ray and Neutron Diffraction. Part 1. Bond Lengths in Organic Compounds, J. Chem. Soc. Perkin Trans.2, (1987) S1–19.

[35] A. Jeyabharathi, M.N. Ponnuswamy, A. Amal Raj, R. Raghunathan, I.A. Razak, A. Usman, S. Chantrapromma, H.-K. Fun, 3-Benzyl-idene-1′-methyl-4′-phenyl-cyclo-hexane-spiro-3′-pyrrolidine-2′-spiro-3″-indoline-2,2″-dione, Acta Cryst. E57 (2001) o901–o903.

[36] J. Suresh, R.S. Kumar, S. Perumal, S. Natarajan. 1'-Methylcyclooctane-1-spiro-3'-pyrrolidine-2'-spiro-3"-indoline-2,2"-dione and 1,1'-dimethylpiperidine-3-spiro-3'-pyrrolidine-2'-spiro-3"-indoline-2",4-dione, Acta Cryst. C63 (2001) o538–o542.

[37] X.-F. Li, Y.-Q. Feng, X.-F. Hu, M. Xu, 1"-Benzyl-5"-benzyl-idene-1'-methyl-4'-phenyl-1H-indole-3-spiro-2'-pyrrolidine-3'-spiro-3"-piperidine-2(3H),3"-dione, Acta Cryst. E59 (2003) o711–o712.

Journal Pre-proof

[38] X.-F. Li, Y.-Q. Feng, X.-F. Hu, M. Xu, 1'-Benzyl-3-(2,6-di-chloro-phenyl)-1''-methyl-4,4''-di-phenyl-oxazole-5(4H)-spiro-3'-piperidine-5'-spiro-3''-pyrrolidine-2''-spiro-3'''-1H-indole-2'''(3'''H),4'-dione benzene hemisolvate, Acta Cryst. E59 (2003) o1280–o1282.

[39] S.J. Wodak, The crystal structure of heliotrine: a pyrrolizidine alkaloid monoester, Acta Cryst. B31 (1975) 569–573.

[40] J. Bernstein, R.E. Davis, L. Shimoni, N.-L. Chang, Patterns in Hydrogen Bonding: Functionality and Graph Set Analysis in Crystals. Angew. Chem. Int. Ed. Engl. 34 (1995) 1555–1573.

[41] R. Kruszynski, T. Sieranski, Can Stacking Interactions Exist Beyond the Commonly Accepted Limits? Cryst. Growth Des. 16 (2016) 587–595.

[42] J.B. Foresman, Æ. Frisch, Exploring Chemistry with Electronic Structure Methods, second ed., Gaussian, Pittsburgh, PA, 1996.

[43] R. Chang, Chemistry, seventh ed., McGraw-Hill, New York, 2001.

[44] B. Kosar, C. Albayrak, Spectroscopic investigations and quantum chemical computational study of (E)-4-methoxy-2-[(p-tolylimino)methyl]phenol, Spectrochim Acta A Mol Biomol Spectrosc. 78 (2011) 160–167.

[45] T.A. Koopmans, About the assignment of wave functions and Eigen values for the individual electrons of an atom, Physica 1 (1993) 104–113.

[46] R.G. Parr, W. Yang, Density-Functional Theory of Atoms and Molecules, Oxford University Press, New York, 1989.

[47] R.G. Parr, L. Von Szentpaly, S.B. Liu, Electrophilicity Index, J. Am. Chem. Soc. 121 (1999) 1922–1924.

[48] R.N. Singh, A. Kumar, R.K. Tiwari, P. Rawat, V.P. Gupta, A combined experimental and quantum chemical (DFT and AIM) study on molecular structure, spectroscopic properties, NBO and multiple interaction analysis in a novel ethyl 4-[2-(carbamoyl)hydrazinylidene]-3,5-dimethyl-1H-pyrrole-2-carboxylate and its dimer, J. Mol. Struct. 1035 (2013) 427-440.

[49] I. Hubert Joe, I. Kostova, C. Ravikumar, M. Amalanathan, S.C. Pinzaru, Theoretical and vibrational spectral investigation of sodium salt of Acenocoumarol, J. Raman Spectrosc. 40 (2009) 1033–1038.

Journal Pre-proof

[50] S. Sebastian, N. Sundaraganesan, The spectroscopic (FT-IR, FT-IR gas phase, FT-Raman and UV) and NBO analysis of 4-Hydroxypiperidine by density functional method. Spectrochim. Acta Part A Mol. Biomol. Spectrosc. 75 (2010) 941–952.

R.S.K.: Conceptualization, writing original draft preparation and supervision; A.I.A.: Investigation; N.A.: Investigation; S.M.S.: Investigation, writing original draft preparation; B.S.K.: Investigation; J.-F.H.: Investigation; V.P.: Investigation, writing original draft preparation; J.S.: Investigation; D.M.A.: Investigation; F.A.A.: Investigation. All authors have read and agreed to the published version of the manuscript.

Declaration of interest

The authors declare no conflict of interest.

Journal Pre-proof